THE JOURNAL OF PHYSICAL CHEMISTRY C

pubs.acs.org/JPCC Article

Adsorption of Chiral Modifiers from Solution onto Supported Platinum Catalysts: The Effect of the Solvent, Other Coadsorbates, and the Support

Yufei Ni, Zihao Wang, Ilkeun Lee, and Francisco Zaera*

Cite This: J. Phys. Chem. C 2020, 124, 7903−7913 Read Online

ACCESS | Metrics & More | Article Recommendations | Supporting Information

ABSTRACT: The adsorption from a solution of s-1-(1-naphthyl)-ethylamine (s-NEA), cinchonidine, and cinchonine on Pt/SiO_2, Pt/Al_2O_3, and a Pt disk was probed in situ by infrared absorption spectroscopy. Adsorption on the supported catalysts shows similar behavior to that seen on flat polycrystalline Pt surfaces, with the adsorption geometry transitioning from the aromatic ring lying close to parallel to the metal surface at low coverages to a more tilted geometry at monolayer saturation. The extent of the adsorption of the chiral modifiers and its degree of irreversibility both vary with the nature of the liquid (CCl_4, toluene, ethanol), tracking solubility. Carbon monoxide can be coadsorbed with s-NEA, a coadsorption that leads to a compression and an increase in ordering of the s-NEA layer (aided by exposing the surface to H_2). In contrast, s-NEA adsorption dominates when competing with quinoline. Finally, a few small differences were seen in the IR spectra of the chiral modifiers adsorbed on Pt/SiO_2 (compared to the other solids) because of the smaller size of the Pt nanoparticles associated with that catalyst. In general, it is crucial to characterize the adsorption of chiral modifiers in situ in the presence of the liquid phase, but the contribution from the catalyst support appears to be minor.

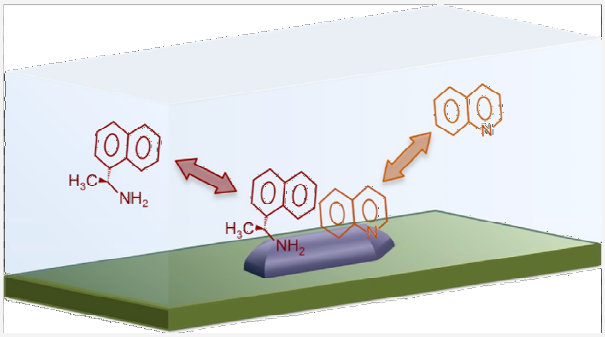

INTRODUCTION

In a quest to improve selectivity in chemical processes involving solid catalysts,[1−7] some scientists have turned to the idea of adding small amounts of molecular modifiers to the reaction mixture.[8−10] The premise is that those modifiers may coadsorb with the reactants on the surface of the catalyst and modify the local environments as to favor specific reaction pathways. This approach is particularly promising in chiral systems, as enantioselectivity requires changes in the transition state of the relevant steps that are too subtle to be accomplished by designing solid catalysts with specific adsorption sites. Instead, the molecular-level modification is attained by the addition of discrete molecules.[11−15] Unfortunately, this idea has so far proven viable only for a limited number of systems and reactions, mainly associated with the hydrogenation of ketoesters promoted either by Ni-based surfaces modified with tartaric acid[16−19] or by Pt catalysts modified with cinchona alkaloids.[20−27]

The extension of the concept of chiral modification in heterogeneous catalysis to a larger family of systems requires a better basic understanding of the surface chemistry involved at a molecular level. A number of research groups, including our own, have dedicated a fair amount of effort to this endeavor with reasonable success,[28−34] but much more remains to be done. One of the fundamental limitations in these studies is that the chiral catalytic systems are quite complex, taking place at liquid−solid interfaces and involving supported heterogeneous catalysts. Simpler models have been used to better be able to address the fundamental chemistry involved, following a so-called modern surface science approach. Well-defined surfaces, single crystal or polycrystalline disks of the main metal in this case, are placed in well-controlled environments, namely, ultrahigh vacuum (UHV) conditions, to be able to use a battery of surface-sensitive techniques such as X-ray photoelectron spectroscopy (XPS),[35] low-energy electron diffraction (LEED),[34−38] scanning tunneling microscopy (STM),[33,34,39,40] temperature-programmed desorption (TPD),[11,33,41,42] and reflection−absorption infrared absorption spectroscopy (RAIRS),[11,33,40−45] to extract molecular details on the adsorption and reactivity of the reactants and modifiers.[14,32,46] This approach has provided much insight into the surface chiral chemistry involved, but is limited by the simplicity of the systems used, which do not include the

Received: February 14, 2020
Revised: March 12, 2020
Published: March 26, 2020

https://dx.doi.org/10.1021/acs.jpcc.0c01309
J. Phys. Chem. C 2020, 124, 7903−7913

solvent present under catalytic conditions (a fact referred to as the "pressure gap"),[47−51] and ignores the characteristics of realistic catalysts, where the metal is present as small nanoparticles (NPs) dispersed on a high-surface-area support, typically an oxide such as silica or alumina (the "materials gap").[48,50−54]

Investigating reactions at solid−liquid interfaces from a surface science perspective is a particular challenge.[55−58] Because many surface-sensitive techniques rely on the use of particles (electrons, ions, atoms) as probes, and because those react strongly with molecules or solids and do not travel far through condensed matter, such techniques are in general not viable to interrogate the solid−liquid interface. A few attempts have been made to adapt spectroscopies such as XPS and X-ray absorption (XAS) to nonvacuum environments,[59−62] but that approach is still in its infancy and cannot yet be used to address general issues regarding the effect of realistic environments on catalysis. More promising is the use of optical spectroscopies such as infrared (IR) absorption[63,64] or Raman,[65] as light is much less affected by liquids and can travel farther through thin liquid films. Most optical spectroscopies are not intrinsically surface-sensitive (nonlinear optical spectroscopies such as second harmonic generation (SHG)[66,67] and sum-frequency generation (SFG)[67−70] being exceptions), but can often be made so by talking advantage of the uniqueness of the surface species or by setting them up in specific geometries.[56,64,71,72]

We in our laboratory have adopted IR absorption spectroscopy, in many of its modalities, to tackle this issue,[64,72−78] and have already reported some results on the adsorption of chiral modifiers onto metal surfaces from liquid solutions.[79−88] However, much of that work has relied on the use of reflection−absorption IR spectroscopy (RAIRS) on flat surfaces, typically polished metal disks; only recently, we have started to extend that work to more realistic supported catalysts.[9,31,89−93] Here, we report on a fairly comprehensive study of the adsorption of chiral modifiers on the surfaces of Pt-based supported catalysts. Emphasis was placed on investigating the effects of key physicochemical parameters such as surface coverage, competition with other adsorbates, and the nature of the solvent and of the catalyst's support. Below we discuss the data and conclusions reached from such work.

EXPERIMENTAL SECTION

The IR absorption spectra from supported Pt catalysts reported here were obtained using a Fourier transform infrared (FTIR) spectrometer (Bruker Tensor 27) and a commercial multiple-bounce attenuated total reflection accessory (ATR, Pike Technologies) equipped with a 60 mm long Ge prism. For the in situ characterization of the adsorption of the catalyst modifiers, a well-defined amount of the catalyst, typically 3 mg, was well dispersed on the surface of the prism, and the ATR cell filled with the pure solvent. The catalyst was preconditioned by bubbling H_2 gas (Liquid Carbonic, 99.995% purity) for 60 min, after which a background IR spectrum was taken. The cell was then exposed to a solution of the modifier, and spectra were taken periodically until surface saturation was reached. Afterward, the cell was flushed with the pure solvent, and additional spectra were acquired to differentiate between weakly and strongly bonded adsorbates. All spectra were acquired by adding 256 scans taken with 4 cm^{-1} resolution, and were ratioed against the reference spectrum recorded at the start of the experiment. A few additional reference spectra are reported in Figure 10: the data for the pure compounds and for their solutions were acquired in transmission mode, using KBr pellets, whereas the traces for the species adsorbed on the Pt disk (already reported in previous publications)[84,90] were obtained using a home-made RAIRS cell.

Adsorption on two commercial Pt-based catalysts was studied here, a 1 wt % Pt/SiO_2 from Sigma-Aldrich and a 1 wt % Pt/Al_2O_3 from Alfa Aesar. Their Pt nanoparticle (NP) dispersions were checked using an FEI Titan Themis 300 scanning transmission electron microscope (STEM); examples of the resulting images and the statistics on the NP size distributions are reported in Figure 1. Emphasis was placed on

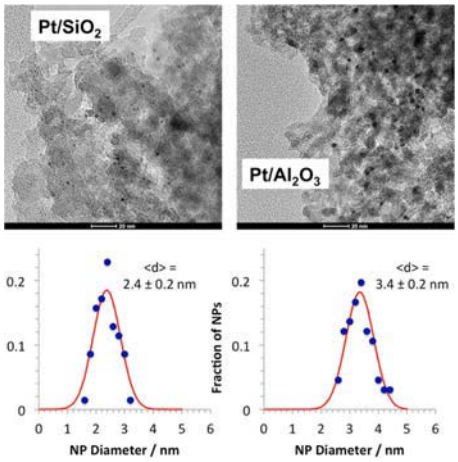

Figure 1. Scanning transmission electron microscopy (STEM) images (top) and Pt NP size distributions obtained for the two catalysts used in this study, namely, Pt/SiO_2 (left) and Pt/Al_2O_3 (right). The scale bars provided in the bottom black strips of the images correspond to 20 nm.

the study of the adsorption of s-1-(1-naphthyl)ethylamine (s-NEA, Sigma-Aldrich, >99% purity), but data are also reported for quinoline (Q, Sigma-Aldrich, 98%), 1-naphthylmethylamine (NMA, Sigma-Aldrich, >97%), cinchonidine (CD, Fluka, 98%), and cinchonidine (CN, Aldrich, 96%). Most solutions were made with carbon tetrachloride (CCl_4, Sigma-Aldrich, 99.9%) as the solvent, but adsorption from solutions made with toluene (Sigma-Aldrich, 99.8%) and with ethanol (Gold Shield, 200 Proof) was also investigated.

RESULTS AND DISCUSSION

s-NEA Uptake. The first set of experiments was directed at exploring the progress of the uptake of s-NEA on the surface of the Pt catalysts. Figures 2 and 3 show IR spectra recorded as a function of time of exposure to a 2 mM solution and as a function of s-NEA concentration, respectively (expanded versions, enlarged in the 1000−1800 cm^{-1} region, are also provided in Figures S1 and S2 in the Supporting Information). Regarding the time evolution of the uptake, the data in Figures 2 and S1 clearly indicate that the IR absorption increases as the exposure time increases, at least within the range of the first two hours. This behavior is typically indicative of a progressive increase in surface coverage, with the caveat that IR intensities can be affected by the adsorption geometry adopted by the adsorbate.[73,94−97] In fact, the changes seen in these and the following figures in terms of the relative intensities of the

https://dx.doi.org/10.1021/acs.jpcc.0c01309
J. Phys. Chem. C 2020, 124, 7903−7913

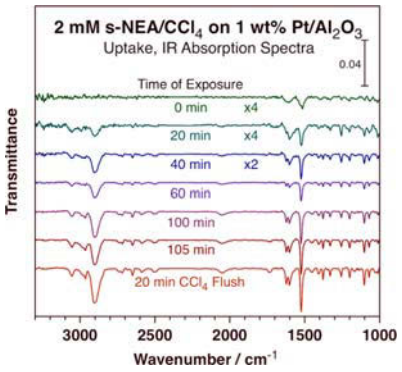

Figure 2. ATR-IR spectra of s-NEA adsorbed on 1 wt % Pt/Al_2O_3 from a 2 mM CCl_4 solution as a function of the time of exposure of the surface to the liquid.

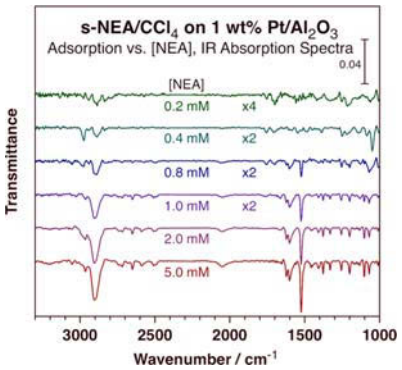

Figure 3. ATR-IR spectra of s-NEA adsorbed on 1 wt % Pt/Al_2O_3 as a function of concentration. CCl_4 was used as the solvent in all cases.

different features of the spectra, together with variations related to shifts in peak position or the appearance of new peaks, point to the fact that the mode of adsorption changes depending on the specific adsorption conditions. This has been observed before, and was used by us in the past to correlate enantioselectivity in CD-modified catalytic hydrogenations with adsorption geometry.[79,86] The adsorption geometry that promotes enantioselectivity is still in dispute, however. Our initial experiments suggested that the flat adsorption seen at low coverages is the one that provides the required chiral environment on the surface for such chiral specificity,[79,86,88] but recent work by the Baiker group has challenged that notion and proposed that the high-coverage tilted species is the one relevant to this catalysis instead.[14,98]

The slow nature of the uptake seen in Figure 2 is most likely due to limitations in mass transport in the system, as the ATR-IR cell is capped with a top plate that constrains the liquid to a space of a few micrometers. Consequently, the time-resolved data may not provide any meaningful information on the kinetics of the adsorption. On the other hand, the traces in Figure 2 can be used to follow the behavior of the s-NEA adsorbate as a function of its surface coverage. All of the traces recorded after the first hour of the uptake show essentially the same features; only the total intensities of the peaks change, approximately doubling in the course of the second hour. It is also seen in Figure 2 that flushing the ATR-IR cell with fresh pure CCl_4 solvent (bottom, brick color trace) does not affect the adsorbed species and that the adsorption from this solvent is irreversible. On the other hand, the spectra obtained within the first hour show some clear differences with respect to the ones acquired at later times. First, even though most peaks are quite weak, there are a few that do stand up in relative terms compared to the intensities seen at high coverages (i.e., at 1253 and 1603 cm^{-1}), and more importantly, there are others (1377 and 1622 cm^{-1}) that display lower intensities than expected. Additionally, the most prominent peak in all of the spectra shifts in position as the relative importance of its two components varies: the signal at 1515 cm^{-1} is quickly overtaken by a more intense and sharp feature at 1524 cm^{-1}.

To better interpret these results, we rely on the assignment of the IR features to specific vibrational modes of the adsorbed s-NEA reported by us in the past.[85,92] The peaks at 1253 and 1603 cm^{-1} prominent in the low-coverage spectra correspond to vibrations within the naphthyl ring, to in-plane ring C−H deformation ($\delta_{ip}(CH)_{ring}$) and in-plane symmetric short-axis ring C−C stretching ($\nu_{ip,sym}(CC)_{ring\text{-}y}$) modes, respectively. The features at 1377 and 1622 cm^{-1} seen at high coverages, on the other hand, are associated with the ethylamine moiety, specifically with symmetric (umbrella) methyl deformation ($\delta_{sym}(CH_3)_{amine}$) and symmetric amine deformation ($\delta_{sym}(NH_2)$) modes, respectively. The fact that the latter are not seen at low coverages can be interpreted using the IR surface selection rule (that states that only vibrational modes with dynamic dipoles having a component perpendicular to the surface plane can be detected in these spectra)[73,94−96] to conclude that the ethylamine moiety is aligned close to parallel to the plane of the surface in the low-coverage extreme. The naphthyl ring must still be slightly tilted (along its long axis), as some of its in-plane vibrational modes are visible from the start of the uptake. Nevertheless, it seems that the s-NEA molecule stands up more, mostly along the short axis, as the surface coverage increases. A degree of ordering is also evident by the absence of some intense features seen in the spectrum of the pure s-NEA, in particular an out-of-plane ring C−H deformation ($\delta_{oop}(CH)_{ring}$) mode at 1167 cm^{-1}.

A similar trend in terms of changes in spectral features, reflecting changes in surface coverage, was seen as a function of the concentration of s-NEA in the solution used in the uptake experiments, with some important differences. The corresponding data are reported in Figures 3 and S2. The first thing that becomes evident from simple inspection of that figure is that the most prominent peak, at 1523 cm^{-1} (due to an in-plane ring C−C stretching mode along the short axis, $\nu_{ip}(CC)_{ring\text{-}y}$), is detected only in solutions with concentrations of 0.8 mM or above. At lower concentrations, the absence of a signal at that frequency indicates that the naphthyl ring is likely to be oriented with its plane parallel to the surface. Only a few features are detectable at the low concentrations, mainly at 1255 ($\tau(NH_2)$) and 1700 and 1760 cm^{-1} (both combination bands) in the low-frequency range, and at 2840, 2894, 2940, and 2975 cm^{-1} in the high-frequency end (all related to $\nu(CH)$ modes within the ethyl moiety); both amine and terminal methyl groups may be sticking out of the surface plane at this stage. For concentrations above 0.8 mM, on the other hand, many peaks are seen, the same as in Figure 2 (after long exposures). Again, a change in adsorption geometry, from a flat aromatic ring configuration to one where the ring is tilted, is seen as the surface coverage is increased (because of a shift in adsorption equilibrium).

The transition in adsorption geometry seen in both cases is highlighted in Figure 4, where the intensities of representative

https://dx.doi.org/10.1021/acs.jpcc.0c01309
J. Phys. Chem. C 2020, 124, 7903−7913

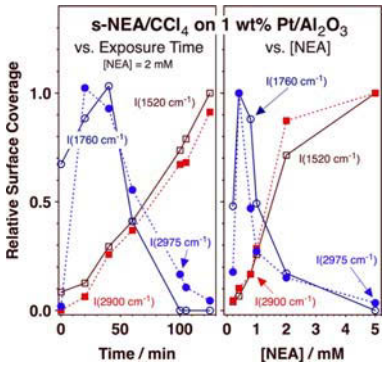

Figure 4. Evolution of the intensities of selected IR peaks for s-NEA adsorbed on a 1 wt % Pt/Al_2O_3 catalyst as a function of time of exposure to a 2 mM solution (left) and of s-NEA concentration (right). The data have been normalized to the highest intensity obtained for each peak.

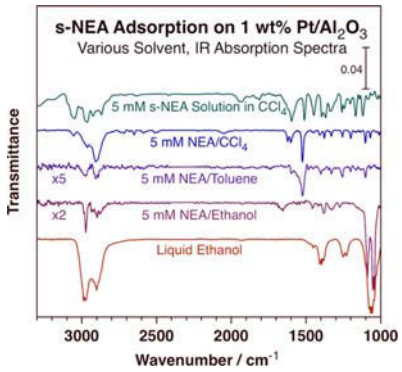

Figure 5. ATR-IR spectra of s-NEA adsorbed from different liquid phases onto a 1 wt % Pt/Al_2O_3 catalyst as a function of the solvent used. Reference spectra are also provided for s-NEA in a CCl_4 solution (top trace, green) and for pure ethanol (bottom, red).

peaks are shown as a function of both exposure time (left panel) and s-NEA concentration in solution (right panel). Two peaks were chosen to follow each of the two surface configurations, 1760 and 2975 cm^{-1} for the low-coverage species, and 1520 and 2900 cm^{-1} for the state seen at high coverages. The development of a tilted adsorbed species at high coverages is quite clear, the coverage of which grows monotonically as either exposure time or solution concentration is increased. The detection of the flatter configuration associated with the low coverages is more difficult to characterize, but can nevertheless be followed in spite of the noisy nature of those spectra. The main conclusion from these studies is that an adsorption geometry transition takes place for s-NEA as a function of coverage on supported Pt catalysts, from an approximately flat alignment of the aromatic ring to a more tilted arrangement, the same as we have reported in the past for CD on flat polycrystalline Pt surfaces.[79,86,88]

In our previous work with the model system, namely, with the flat polycrystalline Pt surfaces, we argued that this adsorption change may justify a change in enantioselectivity during catalytic hydrogenation reactions, and the fact that the same behavior is seen with other chiral modifiers and under more realistic conditions enforces that conclusion. It should be indicated that the IR data presented above only allow us to reach broad conclusions about the orientation of the aromatic ring; they do not provide detailed structural information on the adsorbed species. Moreover, the chiral centers around the modifiers discussed here are flexible and can exist in many rotational configurations; a true picture of the behavior of adsorbed cinchona alkaloids and related molecules such as NEA must take into consideration the interchange that occurs among their possible rotational conformers. Nevertheless, upon complexation with the reactant, the degrees of rotational freedom may be reduced, and specific configurations may dominate and drive the enantioselectivity of the hydrogenation.

Effect of the Solvent on Adsorption. The next set of experiments was aimed at testing the effect of the nature of the solvent on the adsorption of chiral modifiers. Three solvents were tried, namely, carbon tetrachloride, toluene, and ethanol, listed here in order of increasing s-NEA solubility in them. The spectrum for the adsorption of s-NEA from a CCl_4 solution (Figure 5, second from the top, blue, trace) is similar to those reported above, and it indicates strong and irreversible bonding on the surface of the Pt NPs. Detectable, albeit much weaker, adsorption is also seen from the toluene solution (Figure 5, middle, purple, trace). Note in particular the multiplicative factor of 5 used for that trace, needed because of the much lower surface coverage reached in this case under the equilibrium conditions, namely, in the presence of the s-NEA toluene solution. It is also interesting to point out that there are clear differences in the relative intensities, and even in the positions, of some of the IR peaks for adsorbed s-NEA between the CCl_4 and toluene cases. For instance, there is only one broad peak at 1600 cm^{-1} ($\nu_{ip}(CC)_{ring\text{-}y}$) in the spectrum for the adsorption from toluene, similar to the feature seen in solution (Figure 5, top, green, trace), whereas two similar, sharper, and blue-shifted peaks are seen in the CCl_4 case (also seen on Pt disks).[90] One possible interpretation for this difference is that the peak splitting seen in CCl_4 may be due to a supramolecular ordering of the adsorbed layer on the surface (a crystal splitting from pairing of adsorbates in an ordered layer),[31] which may not occur when adsorbing from toluene because of the lower surface coverage, and presumably the larger degree of disorder, reached in that case. In fact, a similar transition was observed with CCl_4 as a function of coverage in Figures 2 and 3. Other differences between the CCl_4 and toluene spectra include the peaks at 1070 cm^{-1} ($\delta_{oop}(CH)_{ring}$) and 1380 cm^{-1} ($\delta_s(CH_3)$) present in the former but not in the latter, indicating that the ethylamine moiety is visible in the first but not in the second case, as well as the stronger signal (in relative terms) for the 2980 cm^{-1} peak, a symmetric in-plane C−H stretching mode within the aromatic ring ($\nu_{ip,s}(CH)$), in toluene. All this is consistent with a flatter and more disordered adsorption from toluene versus a tilted geometry in the case of CCl_4, due to the difference in surface coverage. Alternatively, it is possible for the adsorbed s-NEA to form a complex with the solvent molecules. For instance, the ethylamine group may interact with the OH group of the ethanol, or the rings of the NEA and toluene may facilitate $\pi-\pi$ stacking.

Adsorption of s-NEA from ethanol is weaker still, barely detectable (if at all) in the ATR-IR data. The trace for the ethanol case in Figure 5 (second trace from the bottom, maroon) does display some discernable peaks, but those are most likely due to the direct adsorption of ethanol on the Pt surface. In particular, the strong features at 1043, 1053, and

https://dx.doi.org/10.1021/acs.jpcc.0c01309
J. Phys. Chem. C 2020, 124, 7903−7913

1090 cm^{-1}, due to C−C stretching (ν(CC)) and methyl and ethyl group rocking and twisting ($\rho(CH_3)$, $\tau(CH_2)$) vibrational modes, respectively, and those at 2900 and 2975 cm^{-1} from C−H stretching (ν(CH)) motions, match the peaks seen for liquid ethanol (bottom, red, trace in Figure 5). Some differences are seen between the adsorbed species and the liquid, with peaks in the spectrum for the former at 1275, 1335 1385, 1465, and 1665 cm^{-1} that do not coincide with any specific peaks in the latter, but that is to be expected because of the changing nature of some vibrations upon adsorption on solid surfaces. The adsorbed species may be ethoxy groups rather than ethanol as well. The spectrum reported here for the case of adsorption of s-NEA dissolved in ethanol looks similar (although not exactly identical) to data obtained for ethanol adsorbed onto Pt/Al_2O_3 from the gas phase.[99,100]

An alternative way to probe the role of solvents in the uptake of s-NEA on Pt catalysts, and to also check on the reversibility of such adsorption, is to first deposit a saturated monolayer of the molecule on the surface and then test the ability of different solvents to remove the adsorbed species.[81] Results from this type of experiments are presented in Figure 6. The

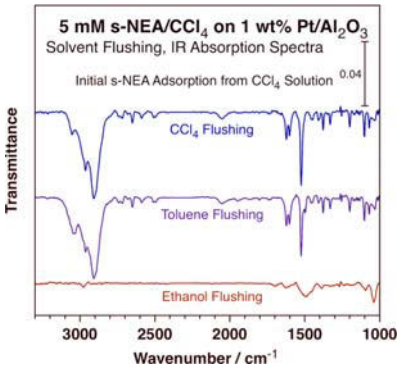

Figure 6. ATR-IR spectra of s-NEA initially adsorbed on Pt/Al_2O_3 from a 5 mM CCl_4 solution (top, blue trace) and after flushing with toluene (middle, purple) and with ethanol (bottom, red).

top trace (blue) in that figure corresponds to the s-NEA layer formed upon adsorption from a 5 mM CCl_4 solution; this layer is similar to what has been reported several times above already. The s-NEA monolayer was then sequentially flushed with pure toluene (middle, purple trace) and with pure ethanol (bottom, red). It is clear that toluene cannot remove the monolayer adsorbed on the Pt NPs of the catalysts, whereas removal is virtually complete upon washing with ethanol. This difference between toluene (and CCl_4, which cannot remove the adsorbed monolayer either; see Figure 2 above) and ethanol relates mainly to the differences in solubility of s-NEA among those solvents. In previous studies, we have shown that solubility plays a key role in determining the extent and reversibility of the adsorption of other chiral modifiers.[3,81,82,86−88] Solubility can in turn be associated with more fundamental physicochemical properties of the solvent such as polarity and dielectric constant,[81,86] and become reflected in changes in both the enthalpic and entropic thermodynamic terms of the adsorption equilibrium constants.[3,88]

Similar flushing experiments were carried out with other chiral modifiers, specifically with CD and CN. The data are reported in Figure 7. The same behavior as with s-NEA was

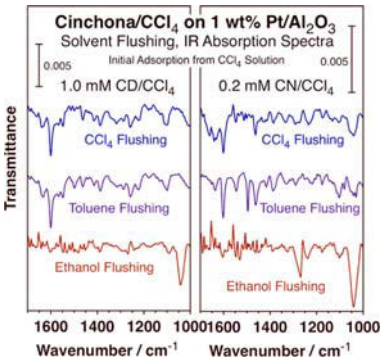

Figure 7. ATR-IR spectra of CD (left) and CN (right) initially adsorbed on Pt/Al_2O_3 from 1 and 0.2 mM CCl_4 solutions, respectively (top, blue trace) and after flushing with toluene (middle, purple) and with ethanol (bottom, red).

observed in these cases as well: the saturated monolayer formed via adsorption from CCl_4 solutions could not be removed with fresh CCl_4 or fresh toluene, but were fully removed with pure ethanol. It should be noted that a few additional peaks are seen in the trace obtained after flushing the adsorbed CN with toluene (Figure 7, right panel, middle, purple trace), but those come from interference due to poor cancelation of the peaks for the solvent. The similarity in behavior among s-NEA, CD, and CN exposed by the results in Figures 6 and 7 suggests a generality in these trends associated with the effect of solvents on the extent and reversibility of the adsorption of chiral modifiers. Similar behavior tendencies were also reported by us for CD and CN on a Pt disk,[76,81] indicating that neither the specific nature of the metal surface nor the support play critical roles in determining the observed solvent trends.

The choice of solvents has been shown in the past to significantly affect the performance of chirally modified catalysts in hydrogenation reactions:[13,19,101−104] high enantioselectivities in the hydrogenation of methyl and ethyl pyruvates have been reported in solvents with intermediate dielectric constants,[101] a result that led to a proposal that an open configuration, helped by those solvents, may be the active form of the chiral modifier.[105] This correlation is yet to be proven universal, but it is worth pointing out that the range of dielectric constants associated with good solvent performance in the catalytic reactions coincides with the higher solubilities seen for the chiral modifiers.[81] It may be that the catalytic activity, and especially enantioselectivity, may depend on the ability of the chiral modifier to easily desorb reversibly from the metal (Pt) surface, perhaps a requirement to better form the modifier:reactant proposed to be active in the chiral promotion.

Coadsorption Systems. A third effect explored in these studies is the potential for different adsorbates to compete for surface sites, which may depend on the relative strength of their adsorption and/or on their solubilities in the liquid phase. We have here identified two types of effects. The first is illustrated by the data in Figure 8 that correspond to the coadsorption of s-NEA with carbon monoxide (dosed in that sequence). Given the small size of CO, it seems that those molecules can still adsorb on the surface of the Pt NPs even after starting with high coverages of s-NEA. Indeed, a distinct peak is seen to grow in the spectra at 2060 cm^{-1} after exposing

https://dx.doi.org/10.1021/acs.jpcc.0c01309
J. Phys. Chem. C 2020, 124, 7903−7913

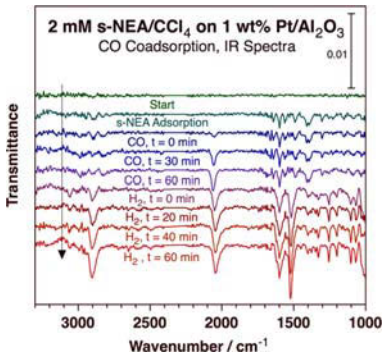

Figure 8. ATR-IR spectra of s-NEA coadsorbed with CO on Pt/Al_2O_3. The dosing was done sequentially, starting with s-NEA (the sequence evolves from top to bottom).

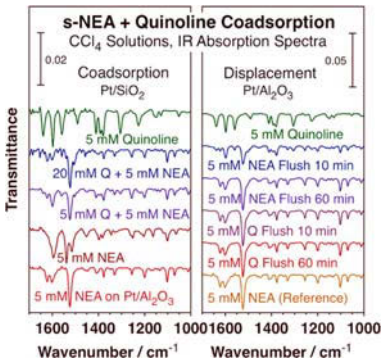

Figure 9. ATR-IR spectra from experiments probing the coadsorption of Q and s-NEA. Left: Data recorded after exposure of a Pt/SiO_2 catalyst to mixed Q + NEA solutions of different compositions. Right: Results from alternating exposure of Pt/Al_2O_3 to Q and s-NEA.

the s-NEA monolayer to CO, starting from the trace after 30 min of CO bubbling. It is worth indicating that at that stage, the peaks corresponding to adsorbed s-NEA are not affected; the new CO molecules seem to simply bind to new surface sites, most likely in the interstices in between the individual molecules of the chiral modifier. On the other hand, additional changes are observed upon switching the CO gas to H_2: The CO peak grows in intensity as it red-shifts, to 2050 cm^{-1}, while the features for s-NEA also grow, some of them notably, and sharpen. The final spectrum, obtained after bubbling H_2 for 60 min, looks like spectra obtained previously for adsorbed s-NEA at high coverages, which adopts a tilted adsorption geometry (see discussion in s-NEA Uptake section). Two things become apparent from these results: (1) the coadsorption of CO with s-NEA compresses the layer of the latter, forcing it to adopt the tilted geometry associated with monolayer saturation; and (2) this rearrangement is aided by H_2. The latter observation is consistent with the fact that the chirally modified catalysts often need to be pretreated with hydrogen for optimum performance.[76,106,107] It should also be mentioned that similar CO-induced monolayer compressing has been seen before with cinchonidine on a flat Pt disk surface.[80] It is somewhat surprising, though, that the same behavior can be seen on small metal NPs, which have much rougher surfaces. It would appear that the ordering and compacting of the monolayers is a localized event, requiring only relatively small terraces of low-Miller-index surfaces.

When the s-NEA monolayer is exposed to solutions of larger molecules such as other chiral modifiers, additional uptake is typically not possible, and only one of the adsorbates ends up dominating on the surface. The data obtained for the coadsorption of s-NEA and Q reported in Figure 9 illustrate this point. Two types of experiments were carried out in these studies: (1) exposure of Pt/SiO_2 to mixed solution with various Q/s-NEA ratios, to directly probe the competitive uptake (Figure 9, left panel) and (2) exposures of Pt/Al_2O_3 sequentially to solutions of pure s-NEA and pure Q, to test the ability of each of those molecules to displace the other from the surface (Figure 9, right panel). Both types of experiments lead to the same conclusion, namely, that s-NEA adsorbs more strongly on the Pt NPs than Q. For one, the tests with the mixed solutions indicate that even with a Q/NEA ratio of 20:5, adsorbed s-NEA dominates the spectra (left panel). In addition, the sequential dosing experiments clearly show that, while s-NEA easily displace adsorbed Q, the opposite is not possible (right panel). Similar behavior has been reported on flat Pt surfaces,[83,87] but, again, the present data extend our previous conclusions to more realistic supported catalysts. Two additional unique details are also worth noting here. First, the spectrum associated with the exposure of the surface to the Q/NEA = 20:5 solution does show some minor peaks from adsorbed Q, indicating that there may be some sites in the Pt NPs still available after saturation with s-NEA; the dominance of adsorbed s-NEA is not as extensive as in the case of flat Pt surfaces.[83] In addition, the spectrum obtained for this Q + s-NEA coadsorbed system, which was obtained with Pt/SiO_2, resembles more closely that of pure s-NEA saturation on Pt/Al_2O_3 than on Pt/SiO_2; note, for instance, the split of the features at about or above 1600 cm^{-1} on the alumina catalyst (bottom traces in both panels of Figure 9), an effect not seen on the silica-based catalyst (second-from-the-bottom trace in the left panel). These differences point to slight changes in the properties of the adsorbed layers with the nature of the catalyst, a point that is discussed in more detail in the next section.

Effect of the Catalyst Support. Finally, we briefly investigated the effect of the nature of the catalyst support. Initial data for this are already available in Figure 9, where the data on the left panel were obtained with Pt/SiO_2 and those on the right panel with Pt/Al_2O_3. In Figure 10, we compare the spectra of saturated monolayers on both catalysts (as well as on a Pt disk, from our previous studies)[84,90] for four molecules, namely (from left to right), Q, NMA, s-NEA, and CD. In general, the uptake on the three types of Pt surfaces is similar and yields IR spectra different from those of the pure compounds or their solutions (in CCl_4). There are nevertheless some subtle differences worth discussing. For Q (Figure 10, left panel), all of the modes seen in the spectra correspond to in-plane stretching or deformation modes within the aromatic ring,[76] which shift significantly upon adsorption. The high intensity of some of the features in the adsorbed species indicates a tilted adsorption geometry, as seen at high coverages with NEA as well (see above), and also with other chiral modifiers. In addition, the spectra from the three Pt surfaces look almost identical (except for the absence of the 1640 cm^{-1} mode on the Pt disk, which we cannot explain at the present time), pointing to the same adsorption mode for quinoline irrespective of the nature of the Pt surface or the support.

https://dx.doi.org/10.1021/acs.jpcc.0c01309
J. Phys. Chem. C 2020, 124, 7903−7913

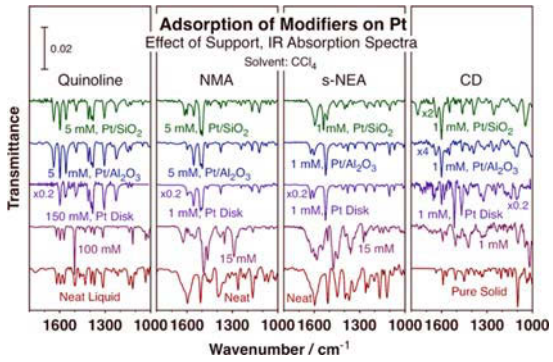

Figure 10. ATR-IR spectra for (from left to right) Q, NMA, s-NEA, and CD, all adsorbed from CCl_4 solutions onto three different Pt samples (from top to bottom): Pt/SiO_2, $PtAl_2O_3$, and a Pt disk. Data are also provided for the pure compounds (bottom traces) and for CCl_4 solutions (second from bottom) for reference. The data for s-NEA (third panel from the left) have been adapted from ref 92 with permission, Copyright 2017 Wiley-VCH Verlag GmbH & Co. KGaA, Weinheim.

Similar arguments can be made for the NMA case (Figure 10, second panel from the left): the three spectra for adsorption on Pt/SiO_2, Pt/Al_2O_3, and a Pt disk are similar among themselves and different from those from the pure or dissolved compound. One thing to note here is that the adsorbed species display distinct features at 1122 and 1378 cm^{-1} not as well resolved in the traces for the free molecule. These peaks can be assigned to motions within the methylamine moiety (possibly rocking, $\rho(CH_2NH_2)$, and methylene deformation, $\delta(CH_2)$, modes), indicating an orientation for that group at an angle from the surface plane. Among the three Pt-containing samples, the main difference in their spectra is the additional peak seen at 1617 cm^{-1} for NMA adsorbed on the Pt/SiO_2 catalyst. As already alluded to before, this may be the result of a crystal field splitting due to a particular local pairing of adsorbates on the surface.[31] It should be indicated that although the spectrum for NMA (and for s-NEA) in the CCl_4 solution looks quite different from the corresponding trace for the pure compound, this is because of interference from the solvent: the strong bands at 1288, 1465, and 1493 cm^{-1} are also seen in the spectrum for pure CCl_4. Once those are removed, the two traces show peaks at approximately the same positions (different from those for the adsorbates).

Once again, the data for s-NEA (Figure 10, third panel from the left) follow similar trends: the three traces for adsorbed s-NEA on the three catalysts are similar, and different from the ones for the pure and dissolved molecule. The latter spectra are also fairly similar to those for NMA, with additional peaks at 1120, 1367, and 1445 cm^{-1} due to the rocking ($\rho(CH_3)$) and symmetric ($\delta_s(CH_3)$, umbrella) and asymmetric ($\delta_{as}(CH_3)$) methyl deformation modes of the extra methyl group in s-NEA compared to NMA. The adsorbed molecules (NMA vs s-NEA), on the other hand, yield fairly different IR spectra, suggesting that, in addition to having an extra methyl group, s-NEA may adsorb with a different geometry on Pt surfaces. It is particularly noteworthy that the main peaks for the in-plane ring breathing modes ($\nu_{ip}(CC)_{ring}$), at approximately 1512 and 1597 cm^{-1} in pure s-NEA, red-shift upon adsorption, a likely consequence of the effect of bonding of the ring to the metal. Moreover, one of those features, the low-frequency one (due to the ring stretching along the short axis) in the case of Pt/SiO_2 and the high-frequency feature (stretching along the long axis) on the Pt disk and on Pt/Al_2O_3, splits into two. This may mean that, although in all cases adsorption is with the aromatic ring in a tilted orientation with respect to the plane of the surface, the axis around which this rotation takes place, and the possible pairing of the adsorbates on the surface, is different on the silica support catalyst. It is also important to recall that in our previous report of adsorption on flat Pt surfaces, we provided evidence suggesting that s-NEA binds to Pt via the nitrogen atom of the amine group.[90] That may also contribute to the differences in the IR spectra discussed here.

Finally, the adsorption of CD (Figure 10, far right panel) is quite similar on Pt/SiO_2 and Pt/Al_2O_3, but somewhat different on the Pt disk: an intense peak is seen in the latter surface but not on the former catalysts at 1516 cm^{-1}, due to the aromatic ring stretching motion along its short axis.[74] In addition, the peak at about 1460 cm^{-1}, from a quinuclidine CH_2 out-of-plane scissoring motion ($\gamma_{oop}(CH_2)_{QN}$), is also more prominent on the disk. It is possible that the rotation of that quinoline ring is different in both cases, possibly because of a larger contribution of the quinoline nitrogen atom to the bonding to Pt on the flat surface. Cinchona alkaloids are relatively big adsorbates, certainly bigger than NEA, and may, therefore, require larger adsorption sites involving multiple-Pt-atom ensembles; those may be more common on flat low-miller-index planes of the metal.

In general, the main trends reported here seem to be general, as they have been seen on different types of surfaces and with different molecules. Adsorption in all cases involves a tilted orientation of the aromatic ring with respect to the metal local plane (at the high coverages tested in Figure 10), even if the azimuthal angle and the proximity of the neighboring adsorbates, which sometimes leads to molecular pairing on the surface, may vary. Because similar behavior was seen before on the surfaces of pure Pt (a polycrystalline disk),[79,84,90] we conclude that it is the metal surface that defines the details of the adsorption and that the porous oxide in the supported catalysts only plays a minor role (if any). Some differences were seen with the catalyst based on silica, but we do not believe that those are due to the nature of the support but rather to a secondary effect from differences in the morphology of the Pt NPs. It should be indicated that no significant adsorption was detected on pure silica or pure alumina under the conditions used here (data not shown). What seems to be relevant is that the Pt NP size distribution is centered around smaller average diameters on SiO_2 vs Al_2O_3 ($\langle d \rangle = 2.4 \pm 0.2$ vs 3.4 ± 0.4 nm, Figure 1). Quite possibly, the smaller NPs exhibit smaller terraces and more edges, kinks, and other defects, and therefore expose a lower number of the flat multi-atom sites typical of flat surfaces. Particle size has been shown in the past to affect activity and enantioselectivity in hydrogenation reactions with chirally modified Pt catalysts, with larger NPs leading to better performance,[108,109] so the effect reported here on adsorption geometry and coverage may be directly correlated to the way the chiral molecules modify the local environment around the catalytic site to promote enantioselectivity. At this stage, though, we view ours as a tentative conclusion in need of further corroboration.

CONCLUSIONS

The adsorption of s-NEA and other related molecules, including Q, NMA, CD, and CN, from solution onto

https://dx.doi.org/10.1021/acs.jpcc.0c01309
J. Phys. Chem. C 2020, 124, 7903−7913

supported Pt catalysts was characterized by in situ IR absorption spectroscopy in ATR mode. These studies extend our previous characterization of the adsorption on flat metal surfaces to consider the behavior on more realistic samples, the same dispersed NP catalysts used to promote hydrogenation reactions. Two catalysts were used, commercial Pt/SiO_2 and Pt/Al_2O_3 samples, the behavior of which was contrasted with the performance of a polycrystalline Pt disk surface. Similar general trends were observed with all of the samples, indicating that the lessons learned from studies on the model Pt disk can be by and large extrapolated to real catalytic conditions. Some slight differences were observed, however, which should be taken into consideration when interpreting kinetic data and when designing new catalysts.

First, it was seen that the uptake of s-NEA on the surfaces of Pt NPs dispersed on typical oxide supports goes through a geometry adsorption transition at intermediate surface coverages, from a configuration with the plane of the aromatic ring close to parallel to that of the metal surface at low coverages to a more tilted arrangement near monolayer saturation. This transition could be clearly seen in the IR spectra both as a function of exposure time (Figures 2 and S1) and of the concentration of s-NEA in the solution (Figures 3 and S2). Figure 4 summarizes this behavior in a semiquantitative way by following the peak intensities of specifically chosen vibrational features, representative of the two adsorption modes.

The effect of the solvent on the adsorption of s-NEA was tested in a couple of ways. In Figure 5, the adsorbed layer in equilibrium with solutions made out of different solvents (CCl_4, toluene, ethanol) was characterized: higher coverages were detected with CCl_4, and virtually no adsorbates could be detected with ethanol. This trend correlates well with the solubility of s-NEA in those solvents. The reversibility of the adsorption was then probed by performing additional experiments where the adsorbed s-NEA monolayer obtained via exposure of the Pt surface to an s-NEA CCl_4 solution was subsequently washed with different pure solvents. Neither CCl_4 nor toluene can remove the adsorbates, whereas ethanol fully cleans the Pt surface (Figure 6). Similar behavior was observed with adsorbed CD and CN (Figure 7).

Coadsorption was also found to affect the uptake of s-NEA on Pt. With small molecules such as CO, it is possible to add them to the surface after exposure to the modifier, even if starting with relatively high s-NEA coverages (Figure 8). The net result is a compression of the s-NEA layer to a more compact, upright, and interacting layer, coadsorbed with surface CO. It was also found that such transition needs to be aided via exposure to H_2, which seems to help with adsorbate mobility. With larger molecules such as Q, coadsorption is more difficult to achieve, and only the more stable adsorbate remains on the surface. Two types of experiments were carried out to test this behavior (Figure 9): (1) exposure of the clean Pt to mixtures of Q and s-NEA (from solution) in different proportions indicated that s-NEA dominates unless a very large excess of Q is used (Figure 9, left panel); and (2) a Q monolayer was seen to be displaced by s-NEA, whereas the opposite displacement of adsorbed s-NEA by Q from solution does not appear to happen (Figure 9, right panel). These two extremes of the effect of coadsorbates on the adsorption of the modifier need to be considered when extending the basic studies on modifier uptake on metal surface to interpret catalytic performance, as the reactant, typically a α-ketoester such as ethyl pyruvate that also needs to adsorb on Pt for its conversion, is a molecule of intermediate size, in between the two tested here (CO and Q). Of course, we have ascribed the coadsorption and displacement phenomena reported above to the size of the adsorbates, but other parameters such as aromaticity, the nature of the functional groups, and bonding modes may play a role as well.

Finally, the effect of the oxide support on the chemistry of the adsorbates was probed by contrasting the characteristics of the monolayers obtained for Q, NMA, s-NEA, and CD on three types of Pt surfaces, namely, on a Pt disk and on Pt/SiO_2- and Pt/Al_2O_3-supported catalysts (Figure 10). In general, each of the four molecules behaves in a similar way on all three solid samples, as the chemistry is mainly dominated by the nature of the Pt metal. Some subtle differences were seen in the case of Pt/SiO_2, but the evidence suggests that such deviation is due to the small size of the Pt NPs in that catalyst: the effect observed is likely to be the result of changes in metal surface structure, not on the physicochemical properties of the oxide or to special interfacial sites. It is also important to reiterate a conclusion already stated in previous work from our lab, and that is that the solvent does alter the properties of the adsorbed chiral modifiers and leads to layers significantly different from those obtained via dosing from the gas phase, in the absence of any liquid.[76,81,84,87,92]

On the basis of the results from all of these studies, we conclude that, in general, it is necessary to include the effect of the liquid phase on the adsorption of chiral modifiers to interpret chiral modification in catalysis, as the solvent induces major changes in the nature of the adsorbate species. In contrast, the new data provided here suggest that the specific characteristics of the metal surface are not as critical and that the support may play no fundamental role at all in defining enantioselectivity. Some changes are seen with very small Pt NPs, but, in general, supported catalysts adsorb these molecules in a way similar to that seen on model solid samples (a Pt disk). All this tracks what has been reported for the enantioselective hydrogenation of α-ketoesters with chirally (NEA, CD, CN) modified Pt catalysts: the catalytic performance varies markedly when different solvents are used, whereas not much difference is seen upon changing the catalyst support as long as the dispersion of the metal NPs is relatively low, that is, as long as the NP size is above a critical value (possibly about $\langle d \rangle \geq 3$ nm).

■ ASSOCIATED CONTENT

Supporting Information

The Supporting Information is available free of charge at https://pubs.acs.org/doi/10.1021/acs.jpcc.0c01309.

Expanded versions of Figures 2 and 3, enlarged in the 1000−1800 cm^{-1} region with peak frequencies for the features (PDF)

■ AUTHOR INFORMATION

Corresponding Author

Francisco Zaera − *Department of Chemistry and UCR Center for Catalysis, University of California, Riverside, California 92521, United States;* orcid.org/0000-0002-0128-7221; Email: zaera@ucr.edu

https://dx.doi.org/10.1021/acs.jpcc.0c01309
J. Phys. Chem. C 2020, 124, 7903−7913

Authors

Yufei Ni − *Department of Chemistry and UCR Center for Catalysis, University of California, Riverside, California 92521, United States*

Zihao Wang − *Department of Chemistry and UCR Center for Catalysis, University of California, Riverside, California 92521, United States*

Ilkeun Lee − *Department of Chemistry and UCR Center for Catalysis, University of California, Riverside, California 92521, United States*

Complete contact information is available at: https://pubs.acs.org/10.1021/acs.jpcc.0c01309

Notes

The authors declare no competing financial interest.

■ ACKNOWLEDGMENTS

Financial assistance for this project was provided by the US National Science Foundation, Division of Chemistry, under grant no. 1854439.

■ REFERENCES

(1) Zaera, F. Outstanding Mechanistic Questions in Heterogeneous Catalysis. *J. Phys. Chem. B* **2002**, *106*, 4043−4052.

(2) Zaera, F. Tuning Selectivity in Hydrocarbon Conversion Catalysis. *J. Mol. Catal. A: Chem.* **2005**, *228*, 21−26.

(3) Zaera, F. Regio, Stereo, and Enantio Selectivity in Hydrocarbon Conversion on Metal Surfaces. *Acc. Chem. Res.* **2009**, *42*, 1152−1160.

(4) Somorjai, G.; Kliewer, C. Reaction Selectivity in Heterogeneous Catalysis: An Invited Review. *React. Kinet. Catal. Lett.* **2009**, *96*, 191−208.

(5) Zaera, F. The New Materials Science of Catalysis: Toward Controlling Selectivity by Designing the Structure of the Active Site. *J. Phys. Chem. Lett.* **2010**, *1*, 621−627.

(6) Zaera, F. The Surface Chemistry of Metal-Based Hydrogenation Catalysis. *ACS Catal.* **2017**, *7*, 4947−4967.

(7) Zhang, L.; Zhou, M.; Wang, A.; Zhang, T. Selective Hydrogenation over Supported Metal Catalysts: From Nanoparticles to Single Atoms. *Chem. Rev.* **2020**, *120*, 683−733.

(8) Schoenbaum, C. A.; Schwartz, D. K.; Medlin, J. W. Controlling the Surface Environment of Heterogeneous Catalysts Using Self-Assembled Monolayers. *Acc. Chem. Res.* **2014**, *47*, 1438−1445.

(9) Weng, Z.; Zaera, F. Increase in Activity and Selectivity in Catalysis via Surface Modification with Self-Assembled Monolayers. *J. Phys. Chem. C* **2014**, *118*, 3672−3679.

(10) Zhao, Y.; Fu, G.; Zheng, N. Shaping the Selectivity in Heterogeneous Hydrogenation by Using Molecular Modification Strategies: Experiment and Theory. *Catal. Today* **2017**, *279*, 36−44.

(11) Lee, I.; Zaera, F. Enantioselectivity of Adsorption Sites Created by Chiral 2-Butanol Adsorbed on Pt(111) Single-Crystal Surfaces. *J. Phys. Chem. B* **2005**, *109*, 12920−12926.

(12) Ernst, K.-H. Molecular Chirality at Surfaces. *Phys. Status Solidi B* **2012**, *249*, 2057−2088.

(13) Meemken, F.; Baiker, A. Recent Progress in Heterogeneous Asymmetric Hydrogenation of C═O and C═C Bonds on Supported Noble Metal Catalysts. *Chem. Rev.* **2017**, *117*, 11522−11569.

(14) Zaera, F. Chirality in Adsorption on Solid Surfaces. *Chem. Soc. Rev.* **2017**, *46*, 7374−7398.

(15) Fang, Y.; Tahara, K.; Ivasenko, O.; Tobe, Y.; De Feyter, S. Structural Insights into the Mechanism of Chiral Recognition and Chirality Transfer in Host−Guest Assemblies at the Liquid−Solid Interface. *J. Phys. Chem. C* **2018**, *122*, 8228−8235.

(16) Izumi, Y. Methods of Asymmetric Synthesis—Enantioselective Catalytic Hydrogenation. *Angew. Chem., Int. Ed.* **1971**, *10*, 871−881.

(17) Keane, M. A.; Webb, G. Asymmetric Hydrogenation of Methyl Acetoacetate Using Ni/SiO2 Modified with Tartaric Acid and Alanine. *J. Mol. Catal.* **1992**, *73*, 91−95.

(18) Osawa, T.; Harada, T.; Takayasu, O. Progress of Enantio-Differentiating Hydrogenation of Prochiral Ketones over Asymmetrically Modified Nickel Catalysts and a Newly Proposed Enantio-Differentiation Model. *Top. Catal.* **2000**, *13*, 155−168.

(19) Studer, M.; Blaser, H. U.; Exner, C. Enantioselective Hydrogenation Using Heterogeneous Modified Catalysts: An Update [Review]. *Adv. Synth. Catal.* **2003**, *345*, 45−65.

(20) Orito, Y.; Imai, S.; Niwa, S.; Nguyen, G. H. Asymmetric Hydrogenation of Methyl Benzoylformate Using Platinum-Carbon Catalysts Modified with Cinchonidine. *J. Synth. Org. Chem. Jpn.* **1979**, *37*, 173−174.

(21) LeBlond, C.; Wang, J.; Liu, J.; Andrews, A. T.; Sun, Y.-K. Highly Enantioselective Heterogeneously Catalyzed Hydrogenation of a-Ketoesters under Mild Conditions. *J. Am. Chem. Soc.* **1999**, *121*, 4920−4921.

(22) Griffiths, S. P.; Johnston, P.; Wells, P. B. Enantioselective Hydrogenation: Chemistry of the Modification of Platinum by Cinchonidine. *Appl. Catal., A* **2000**, *191*, 193−204.

(23) Bartók, M. Heterogeneous Catalytic Enantioselective Hydrogenation of Activated Ketones. *Curr. Org. Chem.* **2006**, *10*, 1533−1567.

(24) Blaser, H.-U. Cinchona Alkaloids as Chirality Transmitters in Metal-Catalyzed Asymmetric Reductions. In *Cinchona Alkaloids in Synthesis and Catalysis: Ligands, Immobilization and Organocatalysis*; Song, C. E., Ed.; John Wiley and Sons: Weinheim, Germany, 2009; pp 11−28.

(25) Ma, Z.; Zaera, F. Chiral Modification of Catalytic Surfaces. In *Design of Heterogeneous Catalysis: New Approaches Based on Synthesis, Characterization, and Modelling*; Ozkan, U. S., Ed.; Wiley-VCH: Weinheim, 2009; pp 113−140.

(26) Tálas, E.; Margitfalvi, J. L. Natural Alkaloids and Synthetic Relatives as Chiral Templates of the Orito's Reaction. *Chirality* **2010**, *22*, 3−15.

(27) Schmidt, E.; Bucher, C.; Santarossa, G.; Mallat, T.; Gilmour, R.; Baiker, A. Fundamental Insights into the Enantioselectivity of Hydrogenations on Cinchona-Modified Platinum and Palladium. *J. Catal.* **2012**, *289*, 238−248.

(28) Bürgi, T.; Baiker, A. Heterogeneous Enantioselective Hydrogenation over Cinchona Alkaloid Modified Platinum: Mechanistic Insights into a Complex Reaction. *Acc. Chem. Res.* **2004**, *37*, 909−917.

(29) Baber, A. E.; Gellman, A. J.; Sholl, D. S.; Sykes, E. C. H. The Real Structure of Naturally Chiral Cu{643}. *J. Phys. Chem. C* **2008**, *112*, 11086−11089.

(30) Demers-Carpentier, V.; Goubert, G.; Masini, F.; Lafleur-Lambert, R.; Dong, Y.; Lavoie, S.; Mahieu, G.; Boukouvalas, J.; Gao, H.; Rasmussen, A. M. H.; et al. Direct Observation of Molecular Preorganization for Chirality Transfer on a Catalyst Surface. *Science* **2011**, *334*, 776−780.

(31) Gordon, A. D.; Karakalos, S.; Zaera, F. Dependence of the Adsorption of Chiral Compounds on Their Enantiomeric Composition. *Surf. Sci.* **2014**, *629*, 3−10.

(32) Gellman, A. J.; Tysoe, W. T.; Zaera, F. Surface Chemistry for Enantioselective Catalysis. *Catal. Lett.* **2015**, *145*, 220−232.

(33) Mahapatra, M.; Burkholder, L.; Garvey, M.; Bai, Y.; Saldin, D. K.; Tysoe, W. T. Enhanced Hydrogenation Activity and Diastereomeric Interactions of Methyl Pyruvate Co-Adsorbed with R-1-(1-Naphthyl)Ethylamine on Pd(111). *Nat. Commun.* **2016**, *7*, No. 12380.

(34) Raval, R. Molecular Assembly at Surfaces: Progress and Challenges. *Faraday Discuss.* **2017**, *204*, 9−33.

(35) Mahapatra, M.; Burkholder, L.; Bai, Y.; Garvey, M.; Boscoboinik, J. A.; Hirschmugl, C.; Tysoe, W. T. Formation of Chiral Self-Assembled Structures of Amino Acids on Transition-Metal Surfaces: Alanine on Pd(111). *J. Phys. Chem. C* **2014**, *118*, 6856−6865.

(36) Mhatre, B. S.; Pushkarev, V.; Holsclaw, B.; Lawton, T. J.; Sykes, E. C. H.; Gellman, A. J. A Window on Surface Explosions: Tartaric Acid on Cu(110). *J. Phys. Chem. C* **2013**, *117*, 7577−7588.
(37) Madden, D. C.; Bentley, M. L.; Jenkins, S. J.; Driver, S. M. On the Role of Molecular Chirality in Amino Acid Self-Organisation on Cu{311}. *Surf. Sci.* **2014**, *629*, 81−87.
(38) Baldanza, S.; Cornish, A.; Nicklin, R. E. J.; Zheleva, Z. V.; Held, G. Surface Chemistry of Alanine on Cu{111}: Adsorption Geometry and Temperature Dependence. *Surf. Sci.* **2014**, *629*, 114−122.
(39) Therrien, A. J.; Lawton, T. J.; Mernoff, B.; Lucci, F. R.; Pushkarev, V. V.; Gellman, A. J.; Sykes, E. C. H. Chiral Nanoscale Pores Created During the Surface Explosion of Tartaric Acid on Cu(111). *Chem. Commun.* **2016**, *52*, 14282−14285.
(40) Gellman, A. J.; Ernst, K.-H. Chiral Autocatalysis and Mirror Symmetry Breaking. *Catal. Lett.* **2018**, *148*, 1610−1621.
(41) Stacchiola, D.; Burkholder, L.; Tysoe, W. T. Enantioselective Chemisorption on a Chirally Modified Surface in Ultrahigh Vacuum: Adsorption of Propylene Oxide on 2-Butoxide-Covered Palladium(111). *J. Am. Chem. Soc.* **2002**, *124*, 8984−8989.
(42) Lee, I.; Zaera, F. Chiral Templating of Surfaces: Adsorption of (S)-2-Methylbutanoic Acid on Pt(111) Single-Crystal Surfaces. *J. Am. Chem. Soc.* **2006**, *128*, 8890−8898.
(43) Lavoie, S.; Laliberté, M.-A.; McBreen, P. H. Adsorption States and Modifier-Substrate Interactions on Pt(111) Relevant to the Enantioselective Hydrogenation of Alkyl Pyruvates in the Orito Reaction. *J. Am. Chem. Soc.* **2003**, *125*, 15756−15757.
(44) Forster, M.; Dyer, M. S.; Persson, M.; Raval, R. Tailoring Homochirality at Surfaces: Going Beyond Molecular Handedness. *J. Am. Chem. Soc.* **2011**, *133*, 15992−16000.
(45) Zeng, Y.; Masini, F.; Rasmussen, A. M. H.; Groves, M. N.; Albert, V.; Boukouvalas, J.; McBreen, P. H. The Most Stable Adsorption Geometries of Two Chiral Modifiers on Pt(111). *Surf. Sci.* **2018**, *676*, 17−22.
(46) Baddeley, C. J.; Jones, T. E.; Trant, A. G.; Wilson, K. E. Fundamental Investigations of Enantioselective Heterogeneous Catalysis. *Top. Catal.* **2011**, *54*, 1348−1356.
(47) Rodriguez, J. A.; Goodman, D. W. High-Pressure Catalytic Reactions over Single-Crystal Metal Surfaces. *Surf. Sci. Rep.* **1991**, *14*, 1−107.
(48) Zaera, F. Probing Catalytic Reactions at Surfaces. *Prog. Surf. Sci.* **2001**, *69*, 1−98.
(49) Tilekaratne, A.; Simonovis, J. P.; López Fagúndez, M. F.; Ebrahimi, M.; Zaera, F. Operando Studies of the Catalytic Hydrogenation of Ethylene on Pt(111) Single Crystal Surfaces. *ACS Catal.* **2012**, *2*, 2259−2268.
(50) Rupprechter, G. Chapter 39: Surface Science Approach to Heterogeneous Catalysis. In *Surface and Interface Science Vol. 5: Solid-Gas Interfaces I*; Wandelt, K., Ed.; Wiley-VCH Verlag GmbH & Co. KGaA: Weinheim, Germany, 2015; Vol. *5*: Solid-Gas Interfaces I; pp 459−528.
(51) Ye, R.; Hurlburt, T. J.; Sabyrov, K.; Alayoglu, S.; Somorjai, G. A. Molecular Catalysis Science: Perspective on Unifying the Fields of Catalysis. *Proc. Natl. Acad. Sci. U.S.A.* **2016**, *113*, 5159−5166.
(52) Goodman, D. W. Model Catalysts: From Imagining to Imaging a Working Surface. *J. Catal.* **2003**, *216*, 213−222.
(53) Freund, H. J. Model Studies in Heterogeneous Catalysis. *Chem.−Eur. J.* **2010**, *16*, 9384−9397.
(54) Zaera, F. Nanostructured Materials for Applications in Heterogeneous Catalysis. *Chem. Soc. Rev.* **2013**, *42*, 2746−2762.
(55) Zaera, F. Surface Chemistry at the Liquid/Solid Interface. *Surf. Sci.* **2011**, *605*, 1141−1145.
(56) Zaera, F. Probing Liquid/Solid Interfaces at the Molecular Level. *Chem. Rev.* **2012**, *112*, 2920−2986.
(57) Tao, F.; Crozier, P. A. Atomic-Scale Observations of Catalyst Structures under Reaction Conditions and During Catalysis. *Chem. Rev.* **2016**, *116*, 3487−3539.
(58) Zaera, F. Probing Liquid/Solid Interfaces at the Molecular Level. In *Surface and Interface Science, Volume 7: Solid-Liquid and Biological Interfaces / Volume 8: Applications of Surface Science*; Wandelt, K., Ed.; Wiley Online Books: Weinheim, Germany, 2020; pp 1−142.
(59) Brown, M. A.; Jordan, I.; Beloqui Redondo, A.; Kleibert, A.; Wörner, H. J.; van Bokhoven, J. A. In Situ Photoelectron Spectroscopy at the Liquid/Nanoparticle Interface. *Surf. Sci.* **2013**, *610*, 1−6.
(60) Wu, C. H.; Weatherup, R. S.; Salmeron, M. B. Probing Electrode/Electrolyte Interfaces in Situ by X-Ray Spectroscopies: Old Methods, New Tricks. *Phys. Chem. Chem. Phys.* **2015**, *17*, 30229−30239.
(61) Karslıoğlu, O.; Nemsak, S.; Zegkinoglou, I.; Shavorskiy, A.; Hartl, M.; Salmassi, F.; Gullikson, E. M.; Ng, M. L.; Rameshan, C.; Rude, B.; et al. Aqueous Solution/Metal Interfaces Investigated in Operando by Photoelectron Spectroscopy. *Faraday Discuss.* **2015**, *180*, 35−53.
(62) Axnanda, S.; Crumlin, E. J.; Mao, B.; Rani, S.; Chang, R.; Karlsson, P. G.; Edwards, M. O. M.; Lundqvist, M.; Moberg, R.; Ross, P.; et al. Using "Tender" X-Ray Ambient Pressure X-Ray Photoelectron Spectroscopy as a Direct Probe of Solid-Liquid Interface. *Sci. Rep.* **2015**, *5*, No. 9788.
(63) Meemken, F.; Müller, P.; Hungerbühler, K.; Baiker, A. Simultaneous Probing of Bulk Liquid Phase and Catalytic Gas-Liquid-Solid Interface under Working Conditions Using Attenuated Total Reflection Infrared Spectroscopy. *Rev. Sci. Instrum.* **2014**, *85*, No. 084101.
(64) Zaera, F. New Advances in the Use of Infrared Absorption Spectroscopy for the Characterization of Heterogeneous Catalytic Reactions. *Chem. Soc. Rev.* **2014**, *43*, 7624−7663.
(65) Chu, W.; LeBlanc, R. J.; Williams, C. T. In-Situ Raman Investigation of Cinchonidine Adsorption on Polycrystalline Platinum in Ethanol. *Catal. Commun.* **2002**, *3*, 547−552.
(66) Heinz, T. F.; Tom, H. W. K.; Shen, Y. R. Determination of Molecular Orientation of Monolayer Adsorbates by Optical Second-Harmonic Generation. *Phys. Rev. A* **1983**, *28*, 1883.
(67) Geiger, F. M. Second Harmonic Generation, Sum Frequency Generation, and $X^{(3)}$: Dissecting Environmental Interfaces with a Nonlinear Optical Swiss Army Knife. *Annu. Rev. Phys. Chem.* **2009**, *60*, 61−83.
(68) Guyot-Sionnest, P.; Superfine, R.; Hunt, J. H.; Shen, Y. R. Vibrational Spectroscopy of a Silane Monolayer at Air/Solid and Liquid/Solid Interfaces Using Sum-Frequency Generation. *Chem. Phys. Lett.* **1988**, *144*, 1−5.
(69) Cremer, P. S.; Su, X.; Somorjai, G. A.; Shen, Y. R. High Pressure Catalytic Processes Studied by Infrared-Visible Sum Frequency Generation. *J. Mol. Catal. A: Chem.* **1998**, *131*, 225−241.
(70) Vidal, F.; Abderrahmane, T. Sum-Frequency Generation Spectroscopy of Interfaces. *Rep. Prog. Phys.* **2005**, *68*, 1095−1127.
(71) Chang, S. C.; Weaver, M. J. In Situ Infrared Spectroscopy at Single-Crystal Metal Electrodes: An Emerging Link between Electrochemical and Ultrahigh-Vacuum Surface Science. *J. Phys. Chem. A* **1991**, *95*, 5391−5400.
(72) Zaera, F. Infrared Absorption Spectroscopy Characterization of Liquid−Solid Interfaces: The Case of Chiral Modification of Catalysts. *Surf. Sci.* **2018**, *669*, 16−24.
(73) Zaera, F. Infrared and Molecular Beam Studies of Chemical Reactions on Solid Surfaces. *Int. Rev. Phys. Chem.* **2002**, *21*, 433−471.
(74) Chu, W.; LeBlanc, R. J.; Williams, C. T.; Kubota, J.; Zaera, F. Vibrational Band Assignments for the Chiral Modifier Cinchonidine: Implications for Surface Studies. *J. Phys. Chem. B* **2003**, *107*, 14365−14373.
(75) Kubota, J.; Ma, Z.; Zaera, F. In-Situ Characterization of Adsorbates in Solid-Liquid Interfaces by Reflection-Absorption Infrared Spectroscopy. *Langmuir* **2003**, *19*, 3371−3376.
(76) Ma, Z.; Lee, I.; Kubota, J.; Zaera, F. In-Situ Characterization of the Adsorption of Cinchona Chiral Modifiers on Platinum Surfaces. *J. Mol. Catal. A: Chem.* **2004**, *216*, 199−207.
(77) Ma, Z.; Zaera, F. In Situ Reflection-Absorption Infrared Spectroscopy at the Liquid-Solid Interface: Decomposition of Organic

https://dx.doi.org/10.1021/acs.jpcc.0c01309
J. Phys. Chem. C 2020, 124, 7903−7913

Molecules on Polycrystalline Platinum Substrates. *Catal. Lett.* **2004**, *96*, 5−12.
(78) Li, J.; Liang, X.; Joo, J. B.; Lee, I.; Yin, Y.; Zaera, F. Mass Transport across the Porous Oxide Shells of Core-Shell and Yolk-Shell Nanostructures in Liquid Phase. *J. Phys. Chem. C* **2013**, *117*, 20043−20053.
(79) Kubota, J.; Zaera, F. Adsorption Geometry of Modifiers as Key in Imparting Chirality to Platinum Catalysts. *J. Am. Chem. Soc.* **2001**, *123*, 11115−11116.
(80) Ma, Z.; Kubota, J.; Zaera, F. The Influence of Dissolved Gases on the Adsorption of Cinchonidine from Solution onto a Platinum Surface: And in-Situ Infrared Spectroscopy Study. *J. Catal.* **2003**, *219*, 404−416.
(81) Ma, Z.; Zaera, F. Role of the Solvent in the Adsorption-Desorption Equilibrium of Cinchona Alkaloids between Solution and a Platinum Surface: Correlations among Solvent Polarity, Cinchona Solubility, and Catalytic Performance. *J. Phys. Chem. B* **2005**, *109*, 406−414.
(82) Zaera, F. The Surface Chemistry of Heterogeneous Catalysis: Mechanisms, Selectivity, and Active Sites. *Chem. Record.* **2005**, *5*, 133−144.
(83) Ma, Z.; Zaera, F. Competitive Chemisorption between Pairs of Cinchona Alkaloids and Related Compounds from Solution onto Platinum Surfaces. *J. Am. Chem. Soc.* **2006**, *128*, 16414−16415.
(84) Ma, Z.; Lee, I.; Zaera, F. Factors Controlling Adsorption Equilibria from Solution onto Solid Surfaces: The Uptake of Cinchona Alkaloids on Platinum Surfaces. *J. Am. Chem. Soc.* **2007**, *129*, 16083−16090.
(85) Lee, I.; Ma, Z.; Kaneko, S.; Zaera, F. 1-(1-Naphthyl)Ethylamine Adsorption on Platinum Surfaces: On the Mechanism of Chiral Modification in Catalysis. *J. Am. Chem. Soc.* **2008**, *130*, 14597−14604.
(86) Mink, L.; Ma, Z.; Olsen, R. A.; James, J. N.; Sholl, D. S.; Mueller, L. J.; Zaera, F. The Physico-Chemical Properties of Cinchona Alkaloids Responsible for Their Unique Performance in Chiral Catalysis. *Top. Catal.* **2008**, *48*, 120−127.
(87) Zaera, F. Chiral Modification of Solid Surfaces: A Molecular View. *J. Phys. Chem. C* **2008**, *112*, 16196−16203.
(88) Lai, J.; Ma, Z.; Mink, L.; Mueller, L. J.; Zaera, F. Influence of Peripheral Groups on the Physical and Chemical Behavior of Cinchona Alkaloids. *J. Phys. Chem. B* **2009**, *113*, 11696−11701.
(89) Hong, J.; Lee, I.; Zaera, F. Cinchona Alkaloids Tethered on Porous Silica as Enantioselective Heterogeneous Catalysts. *Top. Catal.* **2011**, *54*, 1340−1347.
(90) Gordon, A. D.; Zaera, F. Adsorption of 1-(1-Naphthyl)-Ethylamine from Solution onto Platinum Surfaces: Implications for the Chiral Modification of Heterogeneous Catalysts. *Angew. Chem., Int. Ed.* **2013**, *52*, 3453−3456.
(91) Hong, J.; Lee, I.; Zaera, F. Correlated Bifunctionality in Heterogeneous Catalysts: Selective Tethering of Cinchonidine Next to Supported Pt Nanoparticles. *Catal. Sci. Technol.* **2015**, *5*, 680−689.
(92) Ni, Y.; Gordon, A. D.; Tanicala, F.; Zaera, F. Correlation between Chiral Modifier Adsorption and Enantioselectivity in Hydrogenation Catalysis. *Angew. Chem., Int. Ed.* **2017**, *56*, 7963−7966.
(93) Weng, Z.; Zaera, F. Synthesis of Chiral Dendrimer-Encapsulated Nanoparticle (DEN) Catalysts. *Top. Catal.* **2018**, *61*, 902−914.
(94) Greenler, R. G.; Snider, D. R.; Witt, D.; Sorbello, R. S. The Metal-Surface Selection Rule for Infrared Spectra of Molecules Adsorbed on Small Metal Particles. *Surf. Sci.* **1982**, *118*, 415−428.
(95) Parikh, A. N.; Allara, D. L. Quantitative Determination of Molecular Structure in Multilayered Thin Films of Biaxial and Lower Symmetry from Photon Spectroscopies. I. Reflection Infrared Vibrational Spectroscopy. *J. Chem. Phys.* **1992**, *96*, 927−945.
(96) Fan, J.; Trenary, M. Symmetry and the Surface Infrared Selection Rule for the Determination of the Structure of Molecules on Metal Surfaces. *Langmuir* **1994**, *10*, 3649−3657.
(97) Humblot, V.; Pradier, C. M. Chapter 1 - Rairs under Ultrahigh Vacuum Conditions on Metal Surfaces. In *Biointerface Characterization by Advanced IR Spectroscopy*; Pradier, C. M.; Chabal, Y. J., Eds.; Elsevier: Amsterdam, 2011; pp 1−26.
(98) Rodríguez-García, L.; Hungerbühler, K.; Baiker, A.; Meemken, F. The Critical Role of Tilted Cinchona Surface Species for Enantioselective Hydrogenation. *ACS Catal.* **2017**, *7*, 3799−3809.
(99) Raskó, J.; Dömök, M.; Baán, K.; Erdőhelyi, A. FTIR and Mass Spectrometric Study of the Interaction of Ethanol and Ethanol−Water with Oxide-Supported Platinum Catalysts. *Appl. Catal., A* **2006**, *299*, 202−211.
(100) Panagiotopoulou, P.; Verykios, X. E. Mechanistic Aspects of the Low Temperature Steam Reforming of Ethanol over Supported Pt Catalysts. *Int. J. Hydrogen Energy* **2012**, *37*, 16333−16345.
(101) Wehrli, J. T.; Baiker, A.; Monti, D. M.; Blaser, H. U.; Jalett, H. P. Enantioselective Hydrogenation of a-Ketoesters: Influence of Reaction Medium and Conversion. *J. Mol. Catal.* **1989**, *57*, 245−257.
(102) Blaser, H. U.; Jalett, H. P.; Wiehl, J. Enantioselective Hydrogenation of a-Keto Esters with Cinchona-Modified Platinum Catalysts: Effect of Acidic and Basic Solvents and Additives. *J. Mol. Catal.* **1991**, *68*, 215−222.
(103) Sonderegger, O. J.; Ho, G. M.-W.; Bürgi, T.; Baiker, A. Enantioselective Hydrogenation of α-Hydroxyketones over Cinchona-Modified Pt: Influence of Reactant and Modifier Structure. *J. Mol. Catal. A: Chem.* **2005**, *229*, 19−24.
(104) Martin, G.; Mäki-Arvela, P.; Murzin, D. Y.; Salmi, T. Solvent Effects in the Enantioselective Hydrogenation of Ethyl Benzoylformate. *Catal. Lett.* **2013**, *143*, 1051−1060.
(105) Bürgi, T.; Baiker, A. Conformational Behavior of Cinchonidine in Different Solvents: A Combined NMR and Ab Initio Investigation. *J. Am. Chem. Soc.* **1998**, *120*, 12920−12926.
(106) Blaser, H. U.; Jalett, H. P.; Monti, D. M.; Wehrli, J. T. Enantioselective Hydrogenation of a-Keto Esters: Temperature-Programmed Reduction Study of Liquid-Phase Platinum/Alumina Hydrogenation Catalysts. *Appl. Catal.* **1989**, *52*, 19−32.
(107) Mallat, T.; Frauchiger, S.; Kooyman, P. J.; Schürch, M.; Baiker, A. Restructuring During Pretreatment of Platinum/Alumina for Enantioselective Hydrogenation. *Catal. Lett.* **1999**, *63*, 121−126.
(108) Wehrli, J. T.; Baiker, A.; Monti, D. M.; Blaser, H. U. Particle Size Effect on Enantioselective Hydrogenation of Ethyl Pyruvate over Alumina-Supported Platinum Catalyst. *J. Mol. Catal.* **1989**, *49*, 195−203.
(109) Blaser, H. U.; Jalett, H. P.; Monti, D. M.; Baiker, A.; Wehrli, J. T. Enantioselective Hydrogenation of Ethyl Pyruvate: Effect of Catalyst and Modifier Structure. *Stud. Surf. Sci. Catal.* **1991**, *67*, 147−155.

https://dx.doi.org/10.1021/acs.jpcc.0c01309
J. Phys. Chem. C 2020, 124, 7903−7913